Received: 29 December 2023 | Revised: 3 May 2024 | Accepted: 25 June 2024

DOI: 10.1002/hbm.26779

RESEARCH ARTICLE

WILEY

Distinct oscillatory patterns differentiate between segregation and integration processes in perceptual grouping

Gabriel Nascimento Costa[1,2] | Michael Schaum[3] | João Valente Duarte[1,2] | Ricardo Martins[1,2] | Isabel Catarina Duarte[1,2] | João Castelhano[1,2] | Michael Wibral[3,4] | Miguel Castelo-Branco[1,2]

[1]Institute for Biomedical Imaging and Translational Research (CIBIT), University of Coimbra, Coimbra, Portugal

[2]Institute of Nuclear Sciences Applied to Health (ICNAS), University of Coimbra, Coimbra, Portugal

[3]MEG Unit, Brain Imaging Center, Goethe University, Frankfurt/Main, Germany

[4]Campus Institute for Dynamics of Biological Networks, Georg-August University, Göttingen, Germany

Correspondence
Gabriel Nascimento Costa and Miguel Castelo-Branco, Institute for Biomedical Imaging and Translational Research (CIBIT), University of Coimbra, Coimbra, Portugal.
Email: gcosta18@gmail.com and mcbranco@fmed.uc.pt

Present address
Gabriel Nascimento Costa, Trinity College Dublin, Dublin, Ireland.

Funding information
Portuguese Foundation for Science and Technology, FCT, Grant/Award Numbers: 2022.02963.PTDC, CEECIND/00581/2017, DSAIPA/DS/0041/2020, PTDC/PSI-GER/1326/2020, UID/04950B/2020, UID/04950P/2020; BIAL Foundation, Grant/Award Number: 207/16

Abstract

Recently, there has been a resurgence in experimental and conceptual efforts to understand how brain rhythms can serve to organize visual information. Oscillations can provide temporal structure for neuronal processing and form a basis for integrating information across brain areas. Here, we use a bistable paradigm and a data-driven approach to test the hypothesis that oscillatory modulations associate with the integration or segregation of visual elements. Spectral signatures of perception of bound and unbound configurations of visual moving stimuli were studied using magnetoencephalography (MEG) in ambiguous and unambiguous conditions. Using a 2×2 design, we were able to isolate correlates from visual integration, either perceptual or stimulus-driven, from attentional and ambiguity-related activity. Two frequency bands were found to be modulated by visual integration: an alpha/beta frequency and a higher frequency gamma-band. Alpha/beta power was increased in several early visual cortical and dorsal visual areas during visual integration, while gamma-band power was surprisingly increased in the extrastriate visual cortex during segregation. This points to an integrative role for alpha/beta activity, likely from top-down signals maintaining a single visual representation. On the other hand, when more representations have to be processed in parallel gamma-band activity is increased, which is at odds with the notion that gamma oscillations are related to perceptual coherence. These modulations were confirmed in intracranial EEG recordings and partially originate from distinct brain areas. Our MEG and stereo-EEG data confirms predictions of binding mechanisms depending on low-frequency activity for long-range integration and for organizing visual processing while refuting a straightforward correlation between gamma-activity and perceptual binding.

Practitioner Points:

- Distinct neurophysiological signals underlie competing bistable percepts.
- Increased alpha/beta activity correlate with visual integration while gamma correlates with segmentation.
- Ambiguous percepts drive alpha/beta activity in the posterior cingulate cortex.

KEYWORDS
alpha and beta rhythms, gamma activity, intracranial recordings, magnetoencephalography (MEG), oscillations, perceptual binding, stereoEEG

1 | INTRODUCTION

The brain is constantly challenged with interpreting the world based on incomplete and often conflicting sensory signals. This task requires combining information from multiple and often distant brain sources to make sense of the world, a task that relies on contextual information, prior experience, and expectation. The phenomena of ambiguous perception, which can be observed across visual (Hupe & Rubin, 2003; Leopold & Logothetis, 1999), auditory (S. L. Denham et al., 2018; Pressnitzer & Hupe, 2006), and somatosensory domains (Liaci et al., 2016), offer a clear example of our sensory brain's ability to arrive at distinct interpretations from identical stimuli (Long & Toppino, 2004). Continuous perception of ambiguous stimuli usually leads to the phenomenon of perceptual bistability or multistabilty, where perception of two or more possible interpretations alternate in a stochastic manner.

Given their physical constancy, bistable stimuli have been exploited in the study of perception and used to isolate endogenous mechanisms of perceptual decision (Long & Toppino, 2004). These include visual motion perception (Castelo-Branco et al., 2002; Gepshtein & Kubovy, 2007), Gestalt (Keil et al., 1999; Zaretskaya et al., 2013), and several forms of perceptual grouping and scene segmentation (S. Denham et al., 2014; Hupe & Pressnitzer, 2012; Rose & Buchel, 2005). A large body of work on ambiguous and bistable figures centres around neural mechanisms of perceptual binding, that is, the way in which the brain groups or segregates distinct elements and features perceived within, and even across, sensory modalities (Schwartz et al., 2012). We have previously studied binding of different parts of an ambiguous moving figure and found spectral correlates of grouping of distant visual elements and a likely parietal involvement (Costa et al., 2017).

While multistability is dependent on fairly primary neural mechanisms such as adaptation, its susceptibility to effects of expectation and context (Liaw et al., 2022; Long & Toppino, 2004) shows that some of the mechanisms involved lie beyond bottom-up processing (Scocchia et al., 2014). Studies employing ambiguous stimuli reveal a frontoparietal network of brain areas involved in perception, awareness, in reporting one's subjective experience, and, crucially, in solving ambiguity (Brascamp et al., 2018; Sterzer et al., 2009). Overcoming ambiguity thus seems to involve the interplay between bottom-up and top-down signals in early visual cortex and higher cognitive areas (Megumi et al., 2015). Nonetheless, it is not yet understood how areas higher up in the sensory hierarchy interact with earlier visual areas to resolve ambiguity when deciding how to bind distinct visual elements. Moreover, the cortical mechanisms of coding and maintaining distinct stimulus representations that often involve different levels of complexity of a visual scene are also largely unknown.

Building on previous findings on bistable and holistic perception (Duarte et al., 2017; Grassi et al., 2018; Zaretskaya et al., 2013) we used neuromagnetic field imaging to identify the neural signals associated with perceptual binding of distant visual elements (Wallach, 1935; Wuerger et al., 1996). In particular, we aimed to test whether gamma oscillations are associated with perceptual binding under constant physical conditions. Magnetoencephalography (MEG) was recorded while participants viewed ambiguous and unambiguous stimuli that can be perceived as either a bound figure, showing coherent movement and encompassing both hemifields, or as an unbound figure, segmented and with opposing directions of motion in the two hemifields. We employed a data-driven approach to identify the neural signals underlying visual binding of equivalent ambiguous and unambiguous stimuli. In this way, we were able to ascertain the predictions made by proponent theories that explain perceptual binding (Jensen et al., 2014; Liu et al., 2017; Zhang et al., 2019). Independent of the main conditions being studied, we first identified two frequency bands of interest: a lower band corresponding to alpha/beta frequencies, and a higher frequency band within the gamma range. We analysed the activity over these two bands at the source level using beamforming, to assess differences between distinct perceptual outcomes and between different levels of ambiguity. For this we used a 2×2 design that separates correlates of perceptual category (bound vs. unbound) from those of stimulus category (ambiguous vs. unambiguous). During alternating perceptual configurations, over several parietal and occipital areas alpha/beta-band activity was increased when perceiving a single bound configuration while gamma-band activity was increased when perceiving an unbound configuration with two separate figures. We further evaluate this dichotomy in spectral activity using intracranial recordings and confirm the same spectral signatures of visual integration and segregation across the visual cortex. Our results show that alpha/beta and gamma-band activity correlate distinctly with perceptual coherence when interpreting a visual scene. These differences are in line with alpha/beta serving an integrative role and gamma band activity supporting the organisation of multiple perceptual elements.

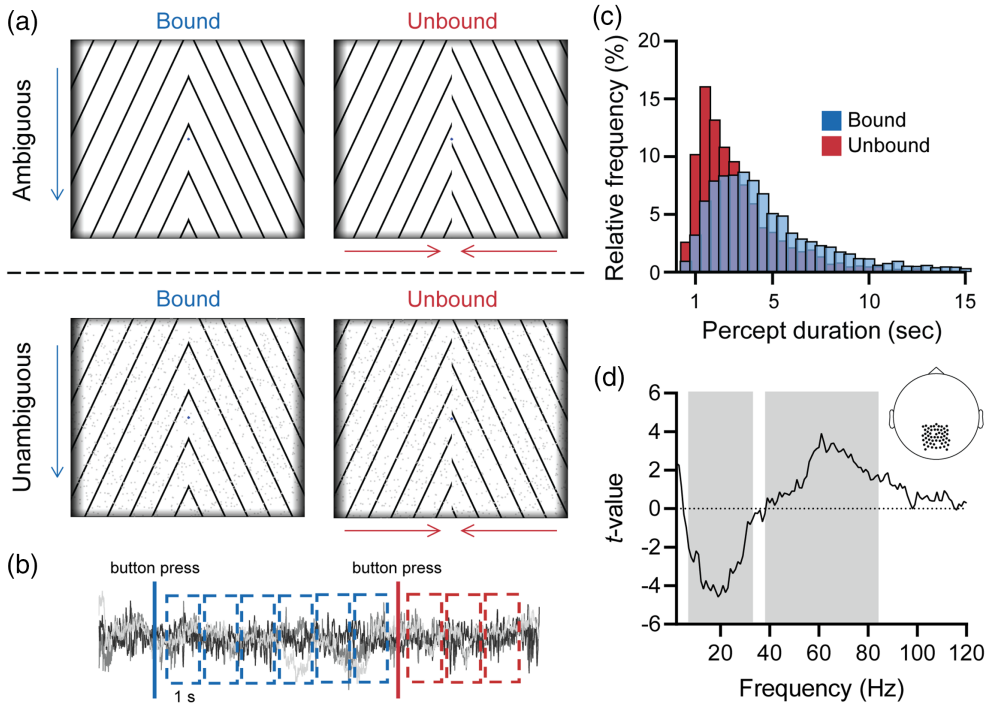

FIGURE 1 Moving stimuli, behavioural data, and spectral activity during task performance. (a) Depiction of the visual stimulus in its ambiguous (top) and unambiguous display (bottom). The two percepts that resulted from continuous viewing of the moving stimulus were a bound configuration (left), with a coherent perception of both visual hemifields and downward motion perception, or an unbound configuration (right), with the left and right sides of the figure appearing to be out-of-phase and inward motion perception. The ambiguous stimulus resulted in bistable perception alternating between the two percepts. Arrows depict the perceived direction of motion. The unambiguous stimuli produced similar percepts but these were driven by the direction of the small moving dots. (b) The experimental design during MEG-acquisition required subjects to continuously indicate their perception by pressing one of two buttons. The moments of perceptual change were identified as such and moments of stable bound or unbound perception were segmented in 1 s epochs for frequency analysis. (c) Histograms of durations of bound and unbound percepts for all participants while viewing the ambiguous stimulus. Perceptual durations followed a typical gamma distribution with instances of bound perception lasting longer than unbound. (d) Sensor level analysis of spectral differences in MEG of baseline vs. task condition. Significant differences were found in occipital sensors for an alpha/beta frequency band (7–33 Hz) and a gamma-frequency band (38–83 Hz; $p < .01$, cluster-based permutation test), the former characterized by a significant decrease and the latter by an increase.

2 | MATERIALS AND METHODS

2.1 | Participants

Twenty-six healthy subjects (14 women; age 20–50 years, mean 28 years) were recruited for the MEG experiment. Three participants were excluded due to excessive head motion during acquisition. All participants had normal or corrected-to-normal vision and no history of neurological or psychiatric disease. All procedures were conducted in accordance with the declaration of Helsinki. Participants gave their informed written consent prior to the experiments and were financially compensated for their time.

2.2 | Stimuli presentation

The ambiguous stimulus was first described by Wallach (1935). Stimulus' properties were as follows: contrast 100%, duty cycle 8%; spatial frequency 0.5 cycle/°, motion speed 6°/s, stimulus size 20° × 22° (vertical × horizontal), and viewing distance 53 cm. Line orientation was changed from a version of the stimulus used in a prior study (Costa et al., 2017) to 65° relative to the x-axis (left-side image) to facilitate unbound perception. Stimulus' borders were smoothed as shown in Figure 1 to reduce the effect of line-terminators influencing motion perception. A central red cross was present as a fixation target at the visual midline to avoid gaze drift. A fully unambiguous stimulus was created by displaying on top of the lines randomly distributed grey dots (600 dots; contrast 10%; visual angle 0.2°), moving at the same speed as the grating pattern and either descending or moving inward. Stimuli were generated in MATLAB (The MathWorks, Inc.) using the Psychophysics Toolbox (Brainard, 1997) and projected on a translucent screen at a refresh rate of 60 Hz.

2.3 | MEG experiment

Participants performed six runs in total, four ambiguous and two unambiguous. Each ambiguous run started with 60 s of a blank screen followed by static stimuli lasting 10 s. After this the stimulus started moving for 60 s during which time the participants were asked to continuously report their perception by pressing and holding one of two buttons (downward motion/bound perception or inward motion/

unbound perception) while maintaining fixation at the central cross. Participants could abstain from reporting any percept in case of doubt. After each block with the stimulus moving the stimulus would stop for 15 s, with participants seeing a static stimulus, and then resume moving for another 60 s block. This was repeated five times for a total of 5 min of ambiguous motion per run. Participants performed an equal number of runs using a different hand to report perception and were given time to rest between runs. For the unambiguous task participants performed two runs lasting 3 min of uninterrupted motion, with unambiguous directions changing randomly every 3–6 s and perceptual reports were given as in the ambiguous task. Participants' responses were recorded using a fibre optic response pad (Photon Control; LUMItouch Response System, BC, Canada). Central fixation during the acquisition session was confirmed with eye-tracking data recorded during acquisition of MEG (1000 Hz sampling rate; Eyelink 1000 Software [SR Research Ottawa, Ontario, Canada]).

2.4 | MEG acquisition and processing

MEG signals were recorded with a 275 channel CTF whole head MEG system (Omega 2005 CIT; VSM Medtech Ltd, Coquitlam, BC, Canada). Data were sampled at 1200 Hz in a synthetic third-order gradiometer configuration and filtered on-line with fourth-order Butterworth with 0.1 high pass and 300 Hz low pass. EKG and vertical and horizontal EOG were recorded with Ag/Ag-Cl-electrodes during the whole task for purposes of artefact rejection. Electrode impedances were kept below 15 kΩ. Head position relative to the MEG channels was measured before each experimental block using three localization coils positioned at the nasion and 1 cm anterior to the tragus of each ear. Runs with head movement exceeding 5 mm were excluded from the analysis. MEG recordings were analysed offline using MATLAB and the Fieldtrip toolbox (Oostenveld et al., 2011).

Datasets were segmented, and epochs containing artefacts and blinks were removed. Independent component analysis was computed on data consisting of all combined conditions and components corresponding to EKG, and muscle artefacts, identified by their scalp topography and spectra, were removed (Helfrich et al., 2016). A notch-filter was applied at 50 and 100 Hz to eliminate powerline noise.

2.5 | Epoch selection and spectral analysis

Epochs of stable ambiguous perception of each perceptual configuration were selected based on each subjects' reports. A period of 500 ms around a button-press was excluded and the remainder of that perceptual state was segmented into nonoverlapping epochs lasting 1 s. Percepts lasting less than 2 s and those immediately after the stimulus started moving (2 s after a moving block started) were not considered for the analysis. Baseline condition epochs lasting 1 s were selected from baseline and from static periods interspersed with ambiguous motion. Epochs of ambiguous and unambiguous motion were pooled in a single condition of active perception and baseline and static conditions were pooled into a baseline condition for the spectral analysis at sensor level. Frequency analysis was carried out using Hanning tapers for frequencies between 2 and 120 Hz (1 Hz frequency resolution) on estimated planar gradient for each sensor location. A dependent-samples permutation t test with cluster-based correction (Maris & Oostenveld, 2007) was used to identify differences in spectral power between baseline and task/perceptual conditions. Threshold was set to $\alpha < .01$, to define cluster-maximum statistics (α_{clust}) and $\alpha < .01$ for comparison with the null distribution of Monte Carlo simulations with 5000 permutations (α_{stat}).

2.6 | Source reconstruction using beamformer

Structural MR images of each participant were obtained with a 3 T Siemens Magnetom Tim Trio scanner (Siemens Medical Solutions, Erlangen, Germany) using a standard T1 3D anatomical magnetization-prepared rapid echo time sequence (3D MPRAGE sequence, 176 slices, $1 \times 1 \times 1$ mm voxel size) for coregistration of MEG data and MR images. We used a frequency domain beamformer, Dynamic Imaging of Coherent sources (Gross et al., 2001), to reconstruct the sources of activity for each frequency of interest identified independently at the sensor level. Frequency analysis of each sensor was carried out using a multitaper method based on Slepian sequences for the frequency bands of interest (the number of tapers was adjusted based on the amount of spectral smoothing for each band). A regular grid in MNI coordinates with 1 cm spaced dipoles was warped to the individual participant's anatomy and placed within a single shell volume conductor model. Two subjects for whom an MRI could not be obtained were analysed using a template MRI with the same resolution (Colin27, 1 mm) (Holmes et al., 1998). Corresponding source locations between subjects were thus aligned based on the matching template source model. A common spatial filter was computed based on individual lead fields using all epochs of interest, bound and unbound, for both tasks, ambiguous and unambiguous to obtain a cross-spectral density matrix. A regularization of 5% was used. These filters were applied for each condition and estimates of source power were compared using cluster-based statistics. We used an extended version of the cluster-based permutations statistics of Fieldtrip toolbox to perform a 2×2 independent groups ANOVA. Briefly, cluster-level statistics were calculated for the two main effects, that is, factors *Perception* and *Ambiguity*, by taking the sum of the F-values within each cluster ($\alpha_{clust} < .01$ for defining cluster based on adjacent voxels as samples) and compared to the distribution of the maximum cluster-level statistics from Monte-Carlo simulations with 5000 permutations for each effect ($\alpha_{stat} < .01$). For the two-main effects, permutations were performed within each factor while the other factor remained constant. After reshuffling assignments F-values were estimated in the resampled data. For the interaction factor, an approximation test was achieved by restricting permutations to occur between one factor and subsequently permuting entire subjects across groups. For a detailed description, see Chan et al. (2021). Peaks were identified as local extrema within significant clusters. All peaks identified are reported in Tables 1 and 2.

TABLE 1 Peak *F*-values of voxels in significant clusters for the alpha/beta band of interest (7–33 Hz) for perception (bound vs. unbound) and task (ambiguous vs. unambiguous) factors and interaction.

		Coordinates (MNI)			
Factor	**Brain region (label)**	***X***	***Y***	***Z***	***F*-value**
Perception	Right prefrontal cortex BA9 (R PFC)	15	50	40	8.84
	Right inferior frontal gyrus BA47 (R IFG)	35	30	−10	13.33
	Right parahippocampal gyrus BA38 (R PHG)	15	0	−40	11.53
	Right inferior temporal gyrus BA20 (R ITG)	45	0	−50	15.40
	Right rolandic cortex BA43 (R RC)	55	−10	20	15.40
	Right primary motor cortex BA4 (R M1)	45	−10	50	12.44
	Left primary motor cortex BA4 (L M1)	−35	−20	40	16.66
	Right supramarginal gyrus BA40 (R SMG)	45	−30	40	12.79
	Right superior temporal gyrus BA22 (R STG)	55	−40	10	14.83
	Left inferior temporal gyrus BA37 (L ITG)	−65	−60	−20	17.37
	Left inferior occipital gyrus BA19 (L IOG)	−25	−90	−20	16.89
	Right anterior superior parietal lobe BA7 (R aSPL)	25	−50	50	10.85
	Left posterior superior parietal lobe BA7 (L pSPL)	−25	−70	30	15.17
	Right superior occipital gyrus BA18/19 (R SOG)	35	−80	10	15.26
	Left superior occipital gyrus BA18/19 (L SOG)	−25	−90	20	15.40
	Left middle occipital gyrus BA18/19 (L MOG)	−45	−90	0	21.35
	Left calcarine cortex BA17 (L CC)	−5	−100	−10	21.27
Ambiguity	Right superior frontal lobe BA9 (R SFL)	25	60	40	10.16
	Right angular gyrus BA39 (R AG)	55	−60	30	9.95
	Right caudate nucleus (R Cau)	5	10	10	12.26
	Right hippocampus (R Hipp)	35	−10	−10	7.98
	Left hippocampus (L Hipp)	−15	−40	0	11.14
	Right superior temporal gyrus BA22 (R STG)	65	−10	0	8.27
	Left intraparietal sulcus BA7 (L IPS)	−25	−70	20	10.78
	Right middle temporal area BA18 (R MT)	65	−70	10	9.46
	Left middle occipital gyrus BA18 (L MOG)	−55	−90	10	12.22
	Left fusiform gyrus BA19 (L FG)	−35	−60	−10	12.63
	Left inferior occipital gyrus BA19 (L IOG)	−35	−90	−10	12.64
	Right lingual gyrus BA18 (R LG)	5	−80	0	14.01
Interaction	Left posterior cingulate cortex BA30 (L PCC)	−5	−40	40	9.61

Note: All peak voxels were obtained from a masked *F*-map of $\alpha_{clust} < .01$, for cluster-maximum statistics, and $\alpha_{stat} < .01$, for the null distribution obtained with Monte Carlo simulations (5000 permutations).
Abbreviation: BA, Brodmann area.

2.7 | sEEG experiment

The participant was a female patient (age 24, age of seizure onset 6, start of Tonic clonic seizures age 21). Depth electrodes were implanted using 3D arrays for the purpose of pre-surgical evaluation of the source of epileptic seizures. The participant performed the visual task on a laptop running the experiment on MATLAB and the Psychtoolbox in a hospital room. Unambiguous stimulus' properties were as described in a previous study (Costa et al., 2017). The participant viewed the unambiguous moving grating and performed a single run lasting 3 min, giving motor reports using a keyboard with their right hand. Two subsequent ambiguous runs were carried out but were discarded from further analysis due to the presence of ictal activity.

2.8 | sEEG recording and analysis

Intracranial EEG was recorded from 128 stereotactically inserted depth electrodes (sEEG) using a Nihon Kohden EEG-21000 system. sEEG were recorded at 1000 Hz sampling rate and band-pass filtered at 0.2 and 200 Hz for further analysis. Electrode localization based on pre-surgical T1-weighted MRI and on postimplantation computerized tomography scan were carried out as described in Stolk et al. (2018). Depth electrodes were re-referenced to a bipolar montage and epochs segmented according to triggers indicating the perceptual condition (bound or unbound). Visual inspection was performed to identify potential interictal- and seizure-related activity. Fast-Fourier transform and Hanning tapers were used for spectral analysis over

TABLE 2 Peak *F*-values of voxels in significant clusters for the gamma band of interest (38–83 Hz) for perception (bound vs. unbound) and task (ambiguous vs. unambiguous) factors.

Factor	Brain region (label)	Coordinates (MNI)			F-value
		X	Y	Z	
Perception	Right premotor area BA6 (R PMA)	5	−20	70	14.17
	Left fronto-orbital cortex BA45 (L FOC)	−45	40	−10	10.55
	Left superior temporal gyrus BA22 (L STG)	−55	−30	0	23.05
	Right posterior superior parietal lobe BA7 (R pSPL)	25	−80	50	14.18
	Left posterior superior parietal lobe BA7 (L pSPL)	−15	−80	50	11.53
	Right inferior occipital gyrus BA18/19 (R IOG)	45	−80	−10	22.80
	Left superior occipital gyrus BA18/19 (L SOG)	−25	−80	10	20.94
	Right superior occipital gyrus BA18/19 (R SOG)	25	−70	20	25.03
	Left insula BA13 (L Ins)	−45	−20	20	12.88
	Left lingual gyrus BA18 (L LG)	−15	50	0	21.83
	Left middle temporal area BA19 (L MT)	−55	−50	10	13.57
	Right middle temporal area BA19 (R MT)	35	−40	10	26.38
Ambiguity	Left primary motor cortex BA4 (L M1)	−25	−10	90	16.23
	Left supplemental motor area BA6 (L SMA)	−5	20	80	17.30
	Right anterior superior parietal lobe BA7 (R aSPL)	15	−50	80	18.63
	Left prefrontal cortex BA10 (L PFC)	−5	70	30	19.29

Note: All peak voxels were obtained from a masked *F*-map of $\alpha_{clust} < .01$, for cluster-maximum statistics, and $\alpha_{stat} < .01$, for the null distribution obtained with Monte Carlo simulations (5000 permutations).
Abbreviation: BA, Brodmann area.

frequencies 2–120 Hz on MATLAB and Fieldtrip. Statistically significant differences in power between conditions were assessed using nonparametric cluster-based statistics.

3 | RESULTS

3.1 | Bistability of competing bound and unbound perception

While viewing the ambiguous moving stimulus participants continuously reported their perception as either bound or unbound. Participants could abstain from reporting in case of uncertainty. This occurred less than 2% of the ambiguous task time (1.8 ± 0.97% of the total task duration), indicating that the bistable figure produced clearly identifiable and mutually exclusive percepts (Figure 1a; top; Supporting Information Video 1). Perceptual durations followed a typical gamma distribution for both percepts (Figure 1c), with bound perception being seemingly more stable with overall longer durations: average perceived duration 7.41 ± 4.42 s for bound and 3.93 ± 1.84 s for unbound (mean ± SD; $p < .0001$, Tukey's multiple comparisons test). The unambiguous stimulus consisted of a similar moving figure with overlayed small dots creating a subtle texture (Figure 1a; bottom; Supporting Information Video 2). This had the effect of producing equivalent bound and unbound perception dependent on the direction of dots guiding the overall motion. Accordingly, participants readily reported perceiving configurations matching the intended ones (mean % matching response = 98.10 ± 3.06%; reaction time = 0.496 ± 0.142 s, mean ± SD). Average perceptual durations were not significantly different between unambiguous percepts (4.62 ± 0.24 s for bound and 4.38 ± 0.26 s for unbound, mean ± SD; n.s., Tukey's multiple comparisons test) or between ambiguous and unambiguous conditions (n.s., two-way ANOVA, Ambiguous vs. Unambiguous).

3.2 | Distinct frequency bands are modulated by the perceptual task

MEG was recorded while participants viewed the moving stimulus and segmented off-line into nonoverlapping epochs consisting of stable perception. Periods of uninterrupted perception of one configuration, that is, between either a perceptual or real change were defined based on the subject's reports (Figure 1b). From these periods, epochs corresponding to bound and unbound perception were obtained and analysed for their spectral content. In order to identify frequency bands of interest in an independent manner, an initial orthogonal analysis was carried out by comparing epochs consisting of active perception, either bound or unbound, with activity over a baseline period (Figure 1d). Differences in spectral power were evident over sensors at parietal and occipital areas and a cluster with significant differences was selected for defining the bands of interest (Figure 1d, inset highlighting selected channels). This revealed two main frequency bands (cluster-based permutation test, $p < .01$) displaying opposite behaviours: a low frequency alpha/beta band (7–33 Hz) which showed a decrease during active engagement in the task and a gamma band (38–83 Hz) showing increased activity during the same task

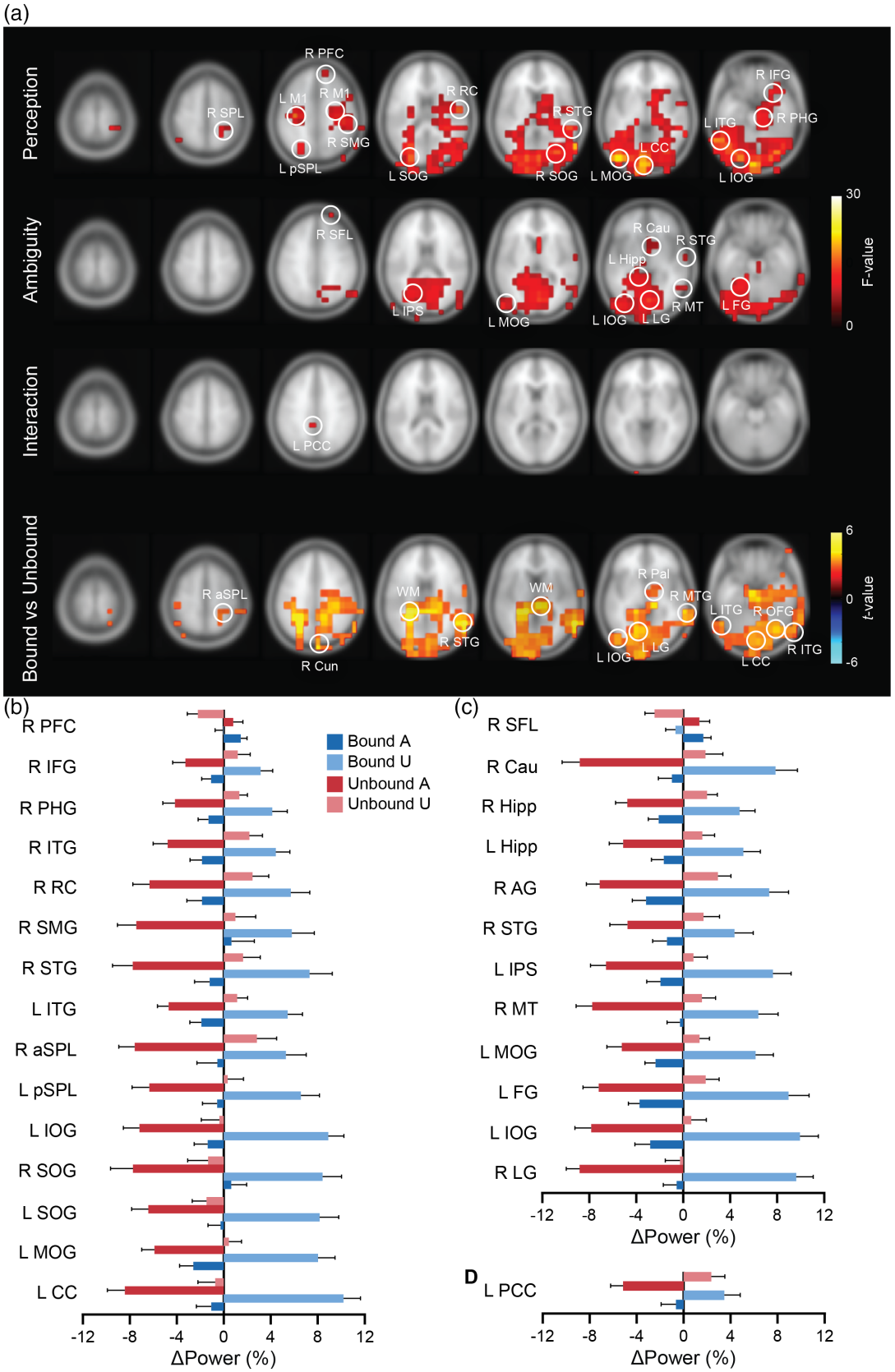

FIGURE 2 Legend on next page.

period. These two frequency bands closely match the alpha/beta and gamma-band activity frequently associated with modulation of cortical excitability and to stimulus processing (Bauer et al., 2014). An independent post hoc analysis of time–frequency responses revealed that these bands are in fact modulated at the time of a perceptual change in ambiguous conditions (Supplementary Information Figure 1). The alpha/beta and gamma bands were thus used in the following analysis of perception-dependent source activity differences. While the current cluster-based statistical analysis did not reveal any separation between alpha and beta frequency bands, these were evident in the average relative difference between spectra (Supporting Information Figure 2) and its sources were also analysed.

3.3 | Alpha/beta activity is increased when perceiving a single moving texture

Perception-related differences in alpha/beta activity (7–33 Hz, frequency limits defined based on an independent baseline vs. task contrast, as described above) were investigated using frequency-domain beamformer source reconstruction. Comparisons were made between conditions of bound and unbound perception (main effect *Perception*) under ambiguous and unambiguous conditions (main effect *Ambiguity*) using a 2 × 2 repeated measures ANOVA. This analysis resulted in *F*-value statistical maps for the main effects of Perception and Ambiguity and an Interaction factor, Perception × Ambiguity. Thus, the cluster-based permutation statistics revealed clusters with significant power differences attributable to perceptual report (bound vs. unbound), stimulus ambiguity level (ambiguous vs. unambiguous stimuli) and to the interaction of perception and ambiguity level (Figure 2). Several regions with significant alpha/beta power differences due to perceptual report were localized in more posterior, mainly visual areas (Figure 2a; top), consisting of a large parieto-occipital cluster, with fewer more anterior areas. Within the broad posterior cluster, peak voxels indicating sources where the Perception effect was stronger could be identified within the calcarine cortex, the middle occipital gyrus, the superior occipital gyrus, and bilaterally in the superior parietal lobe (highlighted in Figure 2a). Peak voxels in ventral areas along the visual pathway were also found in the fusiform gyrus and in the inferior occipital gyrus on the left hemisphere. Despite the predominance of peaks over posterior areas, a few peaks were found more anteriorly including in the right parahippocampal gyrus, the right rolandic cortex, the inferior temporal gyrus, inferior frontal gyrus and in the prefrontal cortex. All peak voxels are listed in Table 1 with coordinates in MNI and approximate anatomical location. A pattern of decreased alpha/beta activity for the unbound perception and increased alpha/beta activity for the bound one was visible in most areas that showed an effect (Figure 2b). Overall, the unambiguous bound percept is most often associated with highest alpha/beta power and the ambiguous unbound percept with lowest, the other two conditions showing intermediate levels of activity over this frequency band. The general effect of perception, controlled in a repeated measures design for attentional effects and for small differences between ambiguous and unambiguous stimuli, appears as a decrease in alpha/beta power when two independent elements are simultaneously perceived and an increase when visual elements are seen as a single entity. The pattern of alpha/beta increase for bound perception and decrease for unbound perception is clear in the overwhelming majority of areas (Figure 2a, top and Figure 2b).

In more detail, for the main effect of Ambiguity differences were observed in more posterior areas related to vision, namely in the right lingual gyrus (Figure 2a middle, *Ambiguity*), left Inferior occipital gyrus, left fusiform gyrus, left middle occipital gyrus, right middle and superior temporal gyrus, and within the right intraparietal sulcus. More anterior peaks were localized to the right angular gyrus and the right superior frontal lobe and outside the neocortex in the right caudate nucleus and bilaterally in the hippocampus (a full list can be found in Table 1). Almost all these areas show a pattern of higher alpha/beta activity for the unambiguous stimuli and lower for the ambiguous one (Figure 2c). Only a single exception to the above pattern was found within the Superior Frontal Lobe, which shows increased alpha/beta activity during the ambiguous task. Lastly, and perhaps most importantly, an interaction effect was observed for the posterior cingulate cortex (PCC; Figure 2a, *Interaction*), an area typically associated with

FIGURE 2 Perception and task-related source activity for alpha/beta band. (a) Top: *F*-maps (Perception, Ambiguity, Interaction) showing areas where each factor of the experimental stimuli had a significant effect over alpha/beta source power (7–33 Hz; two-way ANOVA, one-tailed $p < .01$, cluster-based permutation test). Slices are positioned in −2, 0, +1, +2, +4, +6, +7 cm in *z*, MNI coordinates. Circles highlight peak *F*-values in the statistically significant clusters (see Section 2 for peak selection). Results and coordinates of all peaks are summarized in Table 1. Bottom: *t*-maps for alpha/beta power differences between bound and unbound perception under ambiguous conditions (two-tailed *t* test, $p < .01$, uncorrected). Hot colours represent $Power_{bound} > Power_{unbound}$; cool colours represent $Power_{bound} < Power_{unbound}$. (b) Power differences for percepts (bound and unbound) in ambiguous (A) and unambiguous (U) tasks in voxels with peak significant *F*-value for Perception factor. (c) Power differences for percepts (bound and unbound) in ambiguous and unambiguous tasks in voxels with peak significant *F*-value for Ambiguity factor. (d) Power differences for percepts (bound and unbound) in ambiguous and unambiguous tasks in voxels with peak significant *F*-value for Interaction factor (Perception × Ambiguity). Data are shown as relative difference from baseline condition and are mean ± SEM. Anatomical regions: AG, angular gyrus; aSPL, anterior superior parietal lobe; Cau, caudate nucleus; CC, calcarine cortex; FG, fusiform gyrus; Hipp, hippocampus; IFG, inferior frontal gyrus; IOG, inferior occipital gyrus; IPS, intraparietal sulcus; ITG, inferior temporal gyrus; L, left; LG, lingual gyrus; M1, primary motor cortex, Cun, cuneus; MOG, middle occipital gyrus; MT, middle temporal area; OFG, occipital fusiform gyrus; Pal, pallidum; PCC, posterior cingulate cortex; PFC, prefrontal cortex; PHG, parahippocampal gyrus; pSPL, posterior superior parietal lobe; R, right; RC, Rolandic cortex; SFL, superior frontal lobe; SMG, supramarginal gyrus; SOG, superior occipital gyrus; STG, superior temporal gyrus; WM, white-matter/corpus callosum.

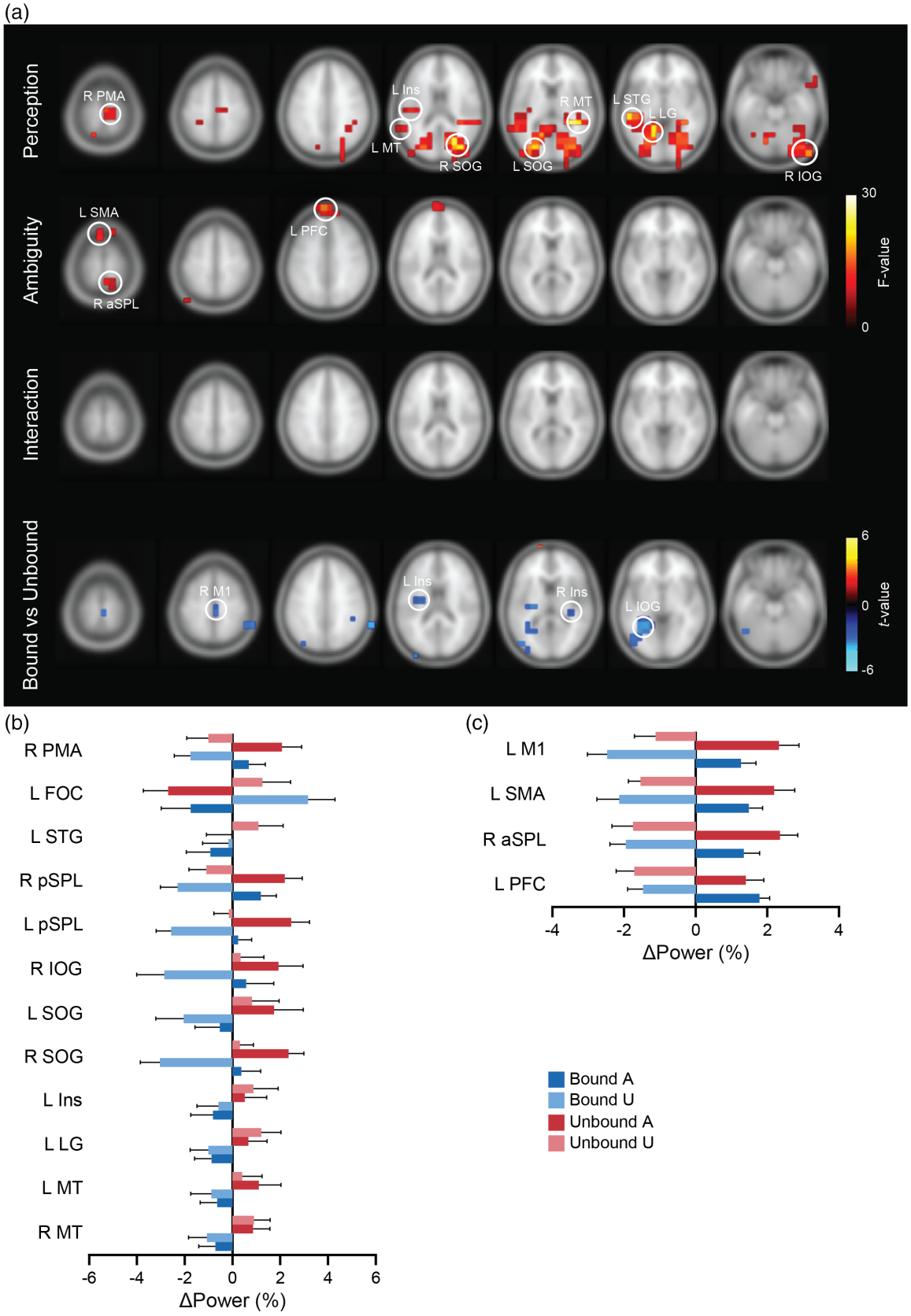

FIGURE 3 Legend on next page.

solving ambiguity (Sun et al., 2017). An interaction effect of Perception × Ambiguity means that this is a difference in activity that distinguishes between bound and unbound reports, but more so in one of the two ambiguity levels. The interaction effect in the PCC consisted of a reduction in power in the unbound condition evident in the ambiguous stimulus but absent in the unambiguous one (Figure 2d). Accordingly, differences in alpha/beta power in the PCC between bound and unbound percepts were only significant for ambiguous percepts (Tukey's post hoc test, bound vs. unbound $p = .0004$ for ambiguous and $p = .485$ for unambiguous; p values adjusted with the Sidak correction).

A direct comparison of the two ambiguous percepts (bound vs. unbound; paired samples t test) shows similar regions as those for the Perception factor in the ANOVA displaying increased alpha/beta activity for the bound perception compared to unbound (Figure 2a; bottom row). Peak voxels are found within both dorsal and ventral visual areas as well as more anteriorly in the temporal cortex. As mentioned above, the employed strategy of selecting frequency bands of interest did not justify a separate analysis of alpha and beta bands. Nonetheless, a source analysis was carried out for individual alpha and beta peaks (8–12 Hz and 16–22 Hz, respectively) selected based on ΔPower peaks (Supplemental Information Figure 2). Even within narrower frequency bands, similar effects in occipital and posterior areas are observed regarding perception (Supplemental Information Figures 3 and 4). This suggests that both frequency bands contribute to the observed power differences within the alpha/beta band of interest.

3.4 | Gamma-band activity is increased across visual areas when perceiving two unbound surfaces

Gamma band source activity (38–83 Hz) analysed for the factor Perception (main effect *Perception*, 2 × 2 repeated measures ANOVA) revealed an effect in more localized clusters than those observed for alpha/beta activity (Figure 3a, top row). Peak voxels appear to comprise several visual areas seemingly outside the immediate primary visual cortex (i.e., BA17, see Table 2), including activity close to bilateral motion sensitive areas in the middle temporal cortex (MT complex) (Huang et al., 2019), and the superior occipital gyrus, likely corresponding to V3a/b (Figure 3a). Local peaks in F-values were also found bilaterally in dorsal areas corresponding to the superior parietal lobes (SPLs; Table 2). In more anterior regions, peak differences were found in the left lingual gyrus, left superior temporal gyrus, and left Insula. Relative power differences for each of the areas identified (Figure 3b) show a clear distinction between the two MT areas, the insula and lingual gyrus compared to other areas with respect to the apparent insensitivity to stimulus features and to ambiguity. These areas show increased gamma power for unbound perception and the presence of dots in the unambiguous stimuli is not reflected in significant effects in their activity. This suggests that the main feature driving gamma-band activity is the overall bound configuration and/or direction of motion. Other regions, including the SPLs and the right premotor area, show small differences between percepts, with most displaying the least gamma-band activity for the unambiguous bound percept and most gamma for the ambiguous unbound percept. For this frequency band and contrast, the SPL peaks appear more posterior than the ones identified for alpha/beta (compare peak coordinates from Table 1 and Table 2).

The F-maps of the main effect of Ambiguity show a small number of areas including premotor and supplementary motor areas, the right SPL and a region within the prefrontal cortex (Figure 3a, middle row; Figure 3c). The main differences in gamma power correspond to increased power for the ambiguous task, possibly reflecting a latent activity during a task with unpredictable perceptual changes. No significant differences were found for the Interaction factor (Figure 3a, third row). Differences in gamma-band activity between the two ambiguous percepts (paired samples t test; Figure 3a, bottom row) reveals lower gamma for the perception of a bound configuration particularly in the left and right Insula and in visual areas (inferior occipital gyrus).

3.5 | Intracranial recordings show bound and unbound perception drive cortical alpha/beta and gamma-band activity within distinct areas

Differences in the power of frequency bands identified in the MEG study seem to arise from several regions. Moreover, in many areas spectral changes correlate with perceptual content rather than with

FIGURE 3 Perception and task-related source activity for gamma band. (a) Top: F-maps (Perception, Ambiguity, Interaction) showing areas where each factor of the experimental stimuli had a significant effect over gamma source power (38–83 Hz; two-way ANOVA, one-tailed $p < .01$, cluster-based permutation test). Slices are positioned in −2, 0, +1, +2, +4, +6, +7 cm in z, MNI coordinates. Circles represent peak F-values in the statistically significant clusters (see Section 2 for peak selection). Results and coordinates of all peaks are summarized in Table 2. No significant cluster was found for the Interaction factor. Bottom: T-maps for gamma power differences between bound and unbound perception under ambiguous conditions (two-tailed t test, $p < .01$, uncorrected). Hot colours represent $\text{Power}_{\text{bound}} > \text{Power}_{\text{unbound}}$; cool colours represent $\text{Power}_{\text{bound}} < \text{Power}_{\text{unbound}}$. (b) Power differences for percepts (bound and unbound) in ambiguous (A) and unambiguous (U) tasks for peak F-value voxels significant for Perception factor. (c) Power differences for percepts (bound and unbound) in ambiguous and unambiguous tasks for peak F-value voxels significant for ambiguity factor. Data are shown as mean ± SEM. Anatomical regions: aSPL, anterior superior parietal lobe; FOC, fronto-orbital cortex; Ins, insula; IOG, inferior occipital gyrus; L, left; LG, lingual gyrus; M1, primary motor cortex; MT, middle temporal area; PFC, prefrontal cortex; PMA, premotor area; pSPL, posterior superior parietal lobe; R, right; SMA, supplemental motor area; SOG, superior occipital gyrus; STG, superior temporal gyrus.

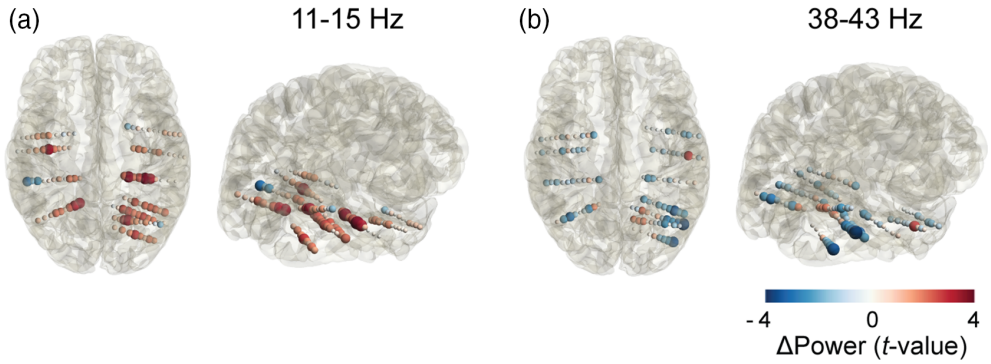

FIGURE 4 Localized sources of percept-related power differences in sEEG. (a) Power difference between bound and unbound perception (unambiguous task) for alpha/beta band (see Section 2 for selection of frequency band in sEEG) represented as point clouds in a translucent mesh of the subject's brain. Electrode's point size is proportional to $|t|$. Hot colours represent $Power_{bound} > Power_{unbound}$; cool colours represent $Power_{bound} < Power_{unbound}$. (b) Power difference between bound and unbound perception for gamma band (see Section 2 for selection of frequency band in sEEG) represented as in (a).

TABLE 3 Perception-related peak differences in sEEG contacts for the low alpha/beta (11–15 Hz) and the gamma (38–43 Hz) frequency bands.

		Coordinates (MNI)			
Frequency band	**Brain region (label)**	***X***	***Y***	***Z***	***t*-Value**
Alpha/beta (11–15 Hz)	Right hippocampus	35	−36	−10	3.86
	Right hippocampus	22	−34	−9	3.66
	Right calcarine cortex/V1 BA17	21	−67	12	3.53
	Left lingual gyrus BA19	−17	−54	−11	3.48
	Left temporal fusiform gyrus BA20	−39	−15	−22	3.45
	Right parahippocampal gyrus BA36	39	−36	−10	3.36
Gamma (38–43 Hz)	Right inferior temporal gyrus BA19	42	−59	−4	−3.26
	Right lateral occipital cortex BA19	40	−82	−6	−3.48
	Right hMT/V5 BA19	49	−69	4	−4.09

Note: The most significant differences were obtained from a paired-sample *t* test and are significant for $\alpha <$ .05 (FDR-corrected, one-tailed).

stimulus features. To clarify whether spectral changes co-occur in the same regions, we analysed human intracranial electrical activity (sEEG) consisting of recordings from similar bound and unbound percepts using an unambiguous display. From the spectrum of all electrodes, two frequency bands showing differences between bound and unbound perception were identified: one in the 11–15 Hz range and another in the 38–43 Hz ($p < .01$, cluster-based permutation test). These bands are narrower than the ones described above for the MEG data, but still fall within the frequency bands identified for the MEG group analysis. The gamma band, in particular, is considerably narrower, around 5 Hz wide, than that identified for the group average, spanning ±20 Hz. This finding is consistent with the interindividual variability of gamma and with increased visual gamma rhythm of subject specific 10 Hz wide gamma bands (Hoogenboom et al., 2006). It is reasonable to expect a similar origin of this gamma-band activity given the similar stimulation and experimental setup. In fact, the same differences found in MEG are reproduced here: an increase in alpha/beta activity during bound perception and an increase in gamma-band activity during unbound perception (Figure 4). Moreover, from the regions sampled with intracranial electrodes, these differences appear in areas that closely match those found in the MEG main effect Perception analysis. As shown in Figure 4a, differences in alpha/beta activity are prominent in electrodes in the early visual cortex, intracalcarine cortex/V1 (BA17; electrodes 71, 72, 73), lingual gyrus (electrodes 116, 117); in the hippocampus and parahippocampal gyrus; and in the occipital fusiform gyrus/V4 (BA18; electrode 63; see Table 3 for a full list of significant differences). Gamma-band activity on the other hand is found increased during unbound perception (Figure 4b), with differences in gamma power evident in the MT area (hMT, BA19; electrodes 54–57), in the inferior lateral occipital cortex (V4, BA19; electrode 67) and inferior temporal gyrus (BA16, electrode 43). Overall, the differences found for alpha/beta and those of gamma-band activity do not show a significant overlap, suggesting activity within these two frequency bands arise for distinct percepts and are modulated in different areas. Pearson's correlation coefficient of alpha/beta and gamma power differences for the electrodes with most significant differences ($p < .01$ for differences in either of the two frequency bands, uncorrected) show no significant correlation ($r = .343$, $p = .12$), as is the case for all electrodes ($r = .129$, $p = .17$).

4 | DISCUSSION

Using MEG and data-driven analysis, we assessed whole-brain spectral activity during distinct perceptual states of visual integration of ambiguous and unambiguous stimuli. Neuromagnetic imaging revealed activity over distinct frequency bands in visual and frontoparietal areas for distinct perceptual outcomes: binding of the moving figure correlated with increased alpha/beta activity while the alternative unbound perception correlated with increased gamma-band activity. Differences within early visual areas were mainly found in the lower frequency band while differences in gamma-band activity were more pronounced over areas further in the visual processing pathway. These findings were replicated in intracortical recordings when contrasting activity between perceptual states corresponding to integration and segmentation of visual motion.

We used state of the art neuromagnetic imaging methods and a 2 × 2 experimental design with an unambiguous control condition to isolate the main effects related to perception, irrespective of its origin (external cue or internal state). We were able to find activity conserved across both conditions and to identify activity unique to the ambiguous condition, located in the left PCC. We also observe a main effect of stimulus-properties (ambiguous vs. unambiguous), which captures influences driven by the physical differences in the stimuli. However, as this main effect is by definition due to physical differences in the stimulus display that were of no interest here, we only discuss it briefly.

An analysis of the spectral content during the visual motion integration task revealed a modulation of alpha/beta and gamma bands, comprising frequencies of 7–33 Hz and 38–83 Hz, respectively. The decreased alpha/beta and increased gamma-band activity when viewing a moving visual stimulus, irrespective of perceptual configuration, could be explained in part as the result of alpha suppression (Klimesch, 2012) and increased activity over visual areas due to greater stimulus complexity and motion strength (Kayser et al., 2003; Siegel et al., 2007). Nonetheless, the perceptually driven differences in the same frequency bands observed in ambiguous and unambiguous conditions suggest that these spectral signals also reflect network interactions and integrative functions (Donner & Siegel, 2011) rather than simply stimulus driven activity or attention (Thut et al., 2006). Spontaneous fluctuations in alpha activity can also affect perceptual experience (Balestrieri & Busch, 2022) and be a driving force in the fluctuations of bistable binding states. The unambiguous task controlled for bistability and for attentional demands, as it presented subjects with unexpected alternating percepts. Perceptual states driven by unambiguous stimuli still resulted in differences over the two frequency bands, which were observed in both MEG and intracranial recordings (sEEG).

Alpha/beta and gamma bands are closely related to neuronal excitability: alpha is typically associated with neuronal inhibition (Klimesch et al., 2007; van Dijk et al., 2008), while both broadband gamma activity and narrow band gamma rhythm positively correlate with spike rate (Ray & Maunsell, 2011). However, recent experimental findings and conceptual models highlight alpha/beta and gamma roles as distinct channels for feedback and feedforward signals across the sensory brain hierarchy (Bastos et al., 2015; Michalareas et al., 2016; van Kerkoerle et al., 2014). Alpha oscillations have been found to modulate neuronal firing within deeper cortical layers and to propagate in the feedback direction, from late to early visual areas (Bollimunta et al., 2008; van Kerkoerle et al., 2014). Similar observations have been made for activity over beta frequencies, with many studies showing feedback signals spanning alpha and beta frequency ranges (Michalareas et al., 2016). It is likely that the cortical mechanisms originating low frequency oscillations within the alpha/beta range play broadly related interareal functions (Fries, 2015; Siegel et al., 2012). Our data-driven strategy to define spectral profiles did not justify a separate selection of narrower frequency bands (Donner & Siegel, 2011), although a post hoc analysis suggests alpha and beta activity may originate from similar regions but in fact play distinct roles in driving perception.

Gamma-band activity on the other hand arises from the more superficial layers of the cortex and is believed to carry feedforward/bottom-up signals (Siegel et al., 2012; van Kerkoerle et al., 2014). In contrast to the current findings, our previous EEG study employing the same perceptual paradigm did not reveal differences in gamma-band activity attributable to different perceptual states (Costa et al., 2017). This disparity could be a result of here using a larger stimulus, which tends to increase gamma oscillations (Ray & Maunsell, 2011), or due to greater sensitivity of MEG and intracranial recordings compared to scalp EEG (Muthukumaraswamy & Singh, 2013).

The two bands modulated during stimulus presentation were also found to undergo modulation related to binding and the number of representations perceived. This binding-related activity was observed accompanying the reports of perceptual changes and was characterized in spatial detail using source analysis. We expected to find embedded in this oscillatory activity signatures of mechanisms structuring sensory information across brain regions (Devia et al., 2021).

4.1 | Alpha/beta activity within the posterior cingulate cortex correlates with endogenous mechanisms of ambiguous perception

Most differences of alpha/beta activity could be attributed to a combination of perceptual states and physical stimuli attributes. Nonetheless, a well-defined source showing an interaction of factors for alpha/beta difference was identified in the PCC. This finding can be explained by the alpha/beta power differences being specific, or at least being highly amplified, in this region for conditions of ambiguity, in comparison to perception resulting from actual physical changes. This mirrors a previous report by Duarte et al. (2017) of an fMRI study with the same paradigm: while perception-related differences in neural activity were found for PCC in ambiguous conditions, such differences were absent when comparing the same percepts in unambiguous conditions. In the current work the 2 × 2 design enabled a direct assessment of this interaction within the PCC

involving endogenous and exogenous signals driving perceptual states. The current findings suggest the PCC separates downstream effects of the percept from the upstream causes for a specific percept, and among these causes the external ones from the internal. The PCC has a dense structural connectivity to many brain regions including the frontoparietal network. This area has been proposed to serve as a cortical hub, coordinating activity between early visual areas and frontoparietal networks, and to play a role in mediating conflict in tasks involving rivalry (Leech et al., 2012; Roy et al., 2017). Even though potentials arising from the cingulate cortex and encoding ambiguity are observed mainly for task-relevant decisions rather than bistability under passive viewing (Sun et al., 2017), in the current study perceptual reports were carried out for both perceptually driven and physical changes. Our results clearly show that alpha/beta power is enhanced in the PCC in conditions of low ambiguity and decreased in conditions of high ambiguity. It remains to be elucidated whether the PCC is involved in awareness of a perceptual state, in conflict resolution or plays an integrative role of visual information. Further insight into the interareal communication during ambiguous perception could result from the analysis of correlated oscillatory activity through functional and directed connectivity measures.

4.2 | Alpha/beta activity is increased by visual integration in posterior parietal cortex and early visual cortex

Perception of the less-complex bound configuration, that is, one moving object, correlated with increased low-frequency power, namely in a frequency band comprising the classical alpha and beta rhythms (Buzsáki, 2006). This was mostly evident in the visual brain and parietal areas in both ambiguous and unambiguous conditions. The early visual cortex receives feedback related to global interpretation of other forms of coherent motion arising from contextual modulation (Muckli et al., 2005; Schwarzkopf et al., 2011) and is found to encode information about unified entities (Fang et al., 2008). The enhanced alpha activity for a coherently moving unified percept in the current paradigm might represent contextual modulation in the early visual cortex carried out by higher order areas. In a temporal coding model proposed by Jensen et al. (2014), this top-down control of the magnitude of alpha can serve to limit the number of representations to be processed. This model describes a mechanism of controlling the flow of information that is dependent on the phase of alpha oscillations and the magnitude of its inhibitory drive, that is, the higher the drive the less elements are processed in an alpha cycle. The current findings support such a temporal phase code for parsing and processing spatially distributed representations, as the increase in alpha/beta power corresponds to perceptual states that require processing an arrangement of fewer visual elements and a less complex scene segmentation. Moreover, the increased alpha/beta activity during visual integration observed across the many visual areas, including in the early visual cortex, parallel findings of conjunctions of visual features being coded as early as in V1 and across the visual brain (Seymour et al., 2009).

Beta and alpha activity have been associated with both perceptual binding and with perceptual stability (Aissani et al., 2014; Mima et al., 2001; Piantoni et al., 2010; Piantoni et al., 2017). Although there is some functional overlap between these bands, there can be distinct contributions for each frequency band. A post hoc source analysis using separate alpha and beta bands provides some support to this idea: both bands show increased activity for a bound percept, but alpha displays more differences related to the ambiguity of the stimulus, while beta activity is mostly modulated by the perceptual content (Supporting Information Figures 3 and 4). Nonetheless, both alpha and beta oscillations have been shown to reflect top-down mechanisms, a potential source of the differences observed here. Top-down signals likely operate similarly in other settings where binding is not involved, although whether or not feedback activity in ambiguous figures is always a result of different forms of binding remains a topic of discussion (Schwartz et al., 2012). Top-down signals from higher to lower visual areas have been proposed to drive a flexible form of perceptual grouping, that is, incremental grouping, that can operate and bind entirely unfamiliar shapes (Roelfsema, 2023). In fact, an increase in information transfer from anterior to posterior areas has been reported recently using a bistable figure in a no-report paradigm (Canales-Johnson et al., 2023), though the source and target regions were not identified. Our results point toward such a mechanism and reveal several of the areas involved.

4.3 | Gamma-band activity is increased during visual segregation and associated with movement perception in extrastriate visual areas

The current findings provide critical evidence that increased gamma power is not a reliable correlate of visual integration (Melloni et al., 2007; Rodriguez et al., 1999), whether it is found in feature specific visual areas, such as MT, or in higher areas along the visual stream. The enhanced gamma-band activity observed in conditions where two distinct surfaces are perceived could thus arise from activity maintaining two internal models, manifesting both in terms of distinct motion-related activity and as a result of surface segregation (Jensen et al., 2014). This scenario is compatible with our results and strongly argues against a straightforward correlation between gamma activity and binding (Tallon-Baudry & Bertrand, 1999). This would be consistent with findings of increased gamma activity associated with retention of feature-conjunction in visual working memory (Honkanen et al., 2015). In line with the current findings, the maintenance of multiple features within a given object would necessarily result in increased neuronal assemblies being recruited, hence increased gamma, whether these features represent a single integrated object or multiple segregated elements. Exploring the relationship between alpha phase and gamma power could further confirm the presence of a temporal code allowing for sequentially sampling two segregated visual elements.

Among the several regions showing differences in gamma-band activity related to distinct perceived configurations, a few display the unique behaviour of seemingly only reacting to global motion perception. Feature selective regions in the MT cortex, likely corresponding bilaterally to hMT+ (Huang et al., 2019; Wang et al., 2015), show differences in gamma power that are sensitive to individual percepts yet agnostic to the stimulus' ambiguity (Figure 3b). Considering the correlation of gamma-band activity and spike rate with BOLD (Logothetis, 2003), the presence of increase gamma power when perception involves two surfaces moving in distinct directions is comparable to findings of increased activity in hMT+ when ambiguous motion is interpreted in more complex configurations (Castelo-Branco et al., 2002). In the current paradigm, however, the ambiguous figure does not involve overlapping gratings, contrary to plaids, and thus alternative motion directions are separated retinotopically. While an overlap of spike activity by direction selective neurons might not be the sole source of the observed gamma differences, segregation of motion in the current paradigm leads to larger motion sensitive clusters being recruited in hMT+ (Sousa et al., 2021). The same pattern of increased gamma-band activity was observed in the insula. It is unlikely that in this area, it emerges from a motion sensitive process, but neural activity in the insula has been proposed as a source of error signals in a predictive model of bistability (Weilnhammer et al., 2017). Interpreted from this angle, a less coherent percept involving distinct surfaces moving one over another and contradicting Gestalt rules could result in higher insula activity.

4.4 | Perceptual integration-related activity is fractioned within the parietal cortex

The current study reveals modulations of different frequency bands that are specific for the perceptual content: bound perception was accompanied by increased alpha/beta activity and reduced gamma-band activity; the opposite pattern was observed for unbound perception. At a glance, most differences were found broadly in similar posterior regions, namely in the occipital and parietal cortices. However, the overlap of peak differences for each frequency band and the correlation between alpha/beta and gamma modulation was low. Thus, no strong evidence was found of competing modes of activity within the same brain areas in response to distinct perceptual configurations, suggesting that each frequency band might subserve distinct, non-mutually exclusive cognitive functions (Honkanen et al., 2015).

Most striking, in the case of differences found particularly in the right SPL the percept-related modulation of alpha/beta activity was localized to a more anterior SPL. On the other hand, the gamma differences localize to a more posterior right SPL (see Tables 1 and 2 for exact MNI coordinates). There is strong evidence that the SPL is responsible for structuring sensory information (Grassi et al., 2018) and activity in the parietal lobe is consistently found in tasks involving bistability (Megumi et al., 2015; Zaretskaya et al., 2013) and perceptual binding (Baumgartner et al., 2013; Costa et al., 2017; Esterman et al., 2007; Zaretskaya & Bartels, 2015). Nonetheless, It has been proposed that there is a functional segregation within the posterior parietal cortex (PPC) (Kanai et al., 2011). Two regions in the right PPC, one more anterior (r-aSPL) and one more posterior in the SPL (r-pSPL), play distinct roles in the process of structuring perception and in bistability (Kanai et al., 2011). More precisely, the picture that emerges from studies of directed connectivity of subregions within the SPL suggest that feedback from r-aSPL is responsible for maintaining a particular percept whereas feedforward signals from r-pSPL are responsible for weakening a percept and precipitating a perceptual switch (Carmel et al., 2010; Kanai & Rees, 2011; Megumi et al., 2015). Within a framework of predictive coding, r-aSPL generates predictions based on sensory evidence and sends top-down signals to r-pSPL and visual areas, while r-pSPL sends bottom-up error signals to r-aSPL. The current findings of increased alpha activity in r-aSPL during visual integration and increased gamma-band activity in r-pSPL during segregation suggest different origins of top-down and bottom-up signals and distinct internal models of visual information. Our results support the role of parietal cortex in guiding local processing in early visual cortex toward perceptual integration by modulating alpha/beta activity (Liu et al., 2017). On the other hand, the increased gamma-band activity arises then from a representation closest to the low-level properties of the stimuli, that is, separated in space and with independent motion.

5 | CONCLUSIONS

We found evidence of two modes of brain activity alternating when perception alternates between bound and unbound configurations of a moving stimulus. The current study provides global coverage of neural responses related to perceptual organization and identifies several regions in the occipital and parietal cortex engaged in solving the cognitive conundrum of ambiguous perception. Our goal was to characterize through spectral analysis cortical population activity responsible for the perception of competing percepts requiring visual binding. These configurations differ in the levels of complexity and likely involve cortical mechanisms of efficient internal representations. We were able to isolate band-limited activity related to binding and to perceptual decision in the alpha/beta and gamma frequency range. This finding builds on and expands the mapping of brain areas involved in perceptual organization by revealing spectral profiles of a network of areas alternating between integrative functions and local encoding of visual information.

AUTHOR CONTRIBUTIONS

Gabriel Nascimento Costa: Designed research, conducted research, analysed data, wrote, and revised manuscript. **Michael Schaum**: Conducted research and revised manuscript. **João Valente Duarte**: Designed research, supported data analysis and revised manuscript. Ricardo Martins: Designed research, conducted research, and revised manuscript. **João Castelhano**: Conducted research, supported data analysis, and revised manuscript. **Isabel Catarina Duarte**: Conducted

research, supported data analysis, and revised manuscript. **Michael Wibral**: Designed research, secured operation of the MEG and MRI equipment and data collection, supported data analysis, and revised manuscript. **Miguel Castelo-Branco**: Designed research, coordinated the project and secured funding, wrote, and revised manuscript.

ACKNOWLEDGEMENTS

This work was supported by the Portuguese Foundation for Science and Technology, FCT, grant IDs: "Projecto Operacional Regional do Centro"—BIGDATIMAGE. Contract grant numbers: CENTRO-01-0145-FEDER-000016, MEDPersyst POCI-01-0145-FEDER-016428, UID/04950B/2020, UID/04950P/2020, DSAIPA/DS/0041/2020, PTDC/PSI-GER/1326/2020, PCIF/SSO/0082/2018, 2022.02963. PTDC and by the BIAL Foundation project 207/16. M. W is employed at the Campus Institute for Dynamics of Biological Networks funded by the Volkswagen Stiftung.

CONFLICT OF INTEREST STATEMENT

The authors declare no conflict of interest.

DATA AVAILABILITY STATEMENT

The data that support the findings of this study are openly available upon reasonable request.

ORCID

Michael Schaum https://orcid.org/0000-0002-6589-4530
João Valente Duarte https://orcid.org/0000-0001-8586-9554
Ricardo Martins https://orcid.org/0000-0001-7184-185X
Miguel Castelo-Branco https://orcid.org/0000-0003-4364-6373

REFERENCES

Aissani, C., Martinerie, J., Yahia-Cherif, L., Paradis, A. L., & Lorenceau, J. (2014). Beta, but not gamma, band oscillations index visual form-motion integration. *PLoS One*, *9*(4), e95541. https://doi.org/10.1371/journal.pone.0095541

Balestrieri, E., & Busch, N. A. (2022). Spontaneous alpha-band oscillations bias subjective contrast perception. *The Journal of Neuroscience*, *42*(25), 5058–5069. https://doi.org/10.1523/JNEUROSCI.1972-21.2022

Bastos, A. M., Vezoli, J., Bosman, C. A., Schoffelen, J. M., Oostenveld, R., Dowdall, J. R., De Weerd, P., Kennedy H., & Fries, P. (2015). Visual areas exert feedforward and feedback influences through distinct frequency channels. *Neuron*, *85*(2), 390–401. https://doi.org/10.1016/j.neuron.2014.12.018

Bauer, M., Stenner, M. P., Friston, K. J., & Dolan, R. J. (2014). Attentional modulation of alpha/beta and gamma oscillations reflect functionally distinct processes. *The Journal of Neuroscience*, *34*(48), 16117–16125. https://doi.org/10.1523/JNEUROSCI.3474-13.2014

Baumgartner, F., Hanke, M., Geringswald, F., Zinke, W., Speck, O., & Pollmann, S. (2013). Evidence for feature binding in the superior parietal lobule. *NeuroImage*, *68*, 173–180. https://doi.org/10.1016/j.neuroimage.2012.12.002

Bollimunta, A., Chen, Y., Schroeder, C. E., & Ding, M. (2008). Neuronal mechanisms of cortical alpha oscillations in awake-behaving macaques. *The Journal of Neuroscience*, *28*(40), 9976–9988. https://doi.org/10.1523/JNEUROSCI.2699-08.2008

Brainard, D. H. (1997). The psychophysics toolbox. *Spatial Vision*, *10*(4), 433–436.

Brascamp, J., Sterzer, P., Blake, R., & Knapen, T. (2018). Multistable perception and the role of the frontoparietal cortex in perceptual inference. *Annual Review of Psychology*, *69*, 77–103. https://doi.org/10.1146/annurev-psych-010417-085944

Buzsáki, G. (2006). *Rhythms of the brain*. Oxford University Press.

Canales-Johnson, A., Beerendonk, L., Chennu, S., Davidson, M. J., Ince, R. A. A., & van Gaal, S. (2023). Feedback information transfer in the human brain reflects bistable perception in the absence of report. *PLoS Biology*, *21*(5), e3002120. https://doi.org/10.1371/journal.pbio.3002120

Carmel, D., Walsh, V., Lavie, N., & Rees, G. (2010). Right parietal TMS shortens dominance durations in binocular rivalry. *Current Biology*, *20*(18), R799–R800. https://doi.org/10.1016/j.cub.2010.07.036

Castelo-Branco, M., Formisano, E., Backes, W., Zanella, F., Neuenschwander, S., Singer, W., & Goebel, R. (2002). Activity patterns in human motion-sensitive areas depend on the interpretation of global motion. *Proceedings of the National Academy of Sciences of the United States of America*, *99*(21), 13914–13919. https://doi.org/10.1073/pnas.202049999

Chan, J. S., Wibral, M., Stawowsky, C., Brandl, M., Helbling, S., Naumer, M. J., M. J., Kaiser, J., & Wollstadt, P. (2021). Predictive coding over the lifespan: Increased reliance on perceptual priors in older adults-a magnetoencephalography and dynamic causal modeling study. *Frontiers in Aging Neuroscience*, *13*, 631599. https://doi.org/10.3389/fnagi.2021.631599

Costa, G. N., Duarte, J. V., Martins, R., Wibral, M., & Castelo-Branco, M. (2017). Interhemispheric binding of ambiguous visual motion is associated with changes in beta oscillatory activity but not with gamma range synchrony. *Journal of Cognitive Neuroscience*, *29*(11), 1829–1844. https://doi.org/10.1162/jocn_a_01158

Denham, S., Bohm, T. M., Bendixen, A., Szalardy, O., Kocsis, Z., Mill, R., & Winkler, I. (2014). Stable individual characteristics in the perception of multiple embedded patterns in multistable auditory stimuli. *Frontiers in Neuroscience*, *8*, 25. https://doi.org/10.3389/fnins.2014.00025

Denham, S. L., Farkas, D., van Ee, R., Taranu, M., Kocsis, Z., Wimmer, M., Carmel, D., & Winkler, I. (2018). Similar but separate systems underlie perceptual bistability in vision and audition. *Scientific Reports*, *8*(1), 7106. https://doi.org/10.1038/s41598-018-25587-2

Devia, C., Concha-Miranda, M., & Rodriguez, E. (2021). Bi-stable perception: Self-coordinating brain regions to make-up the mind. *Frontiers in Neuroscience*, *15*, 805690. https://doi.org/10.3389/fnins.2021.805690

Donner, T. H., & Siegel, M. (2011). A framework for local cortical oscillation patterns. *Trends in Cognitive Sciences*, *15*(5), 191–199. https://doi.org/10.1016/j.tics.2011.03.007

Duarte, J. V., Costa, G. N., Martins, R., & Castelo-Branco, M. (2017). Pivotal role of hMT+ in long-range disambiguation of interhemispheric bistable surface motion. *Human Brain Mapping*, *38*(10), 4882–4897. https://doi.org/10.1002/hbm.23701

Esterman, M., Verstynen, T., & Robertson, L. C. (2007). Attenuating illusory binding with TMS of the right parietal cortex. *NeuroImage*, *35*(3), 1247–1255. https://doi.org/10.1016/j.neuroimage.2006.10.039

Fang, F., Kersten, D., & Murray, S. O. (2008). Perceptual grouping and inverse fMRI activity patterns in human visual cortex. *Journal of Vision*, *8*(7), 2. https://doi.org/10.1167/8.7.2

Fries, P. (2015). Rhythms for cognition: Communication through coherence. *Neuron*, *88*(1), 220–235. https://doi.org/10.1016/j.neuron.2015.09.034

Gepshtein, S., & Kubovy, M. (2007). The lawful perception of apparent motion. *Journal of Vision*, *7*(8), 9. https://doi.org/10.1167/7.8.9

Grassi, P. R., Zaretskaya, N., & Bartels, A. (2018). A generic mechanism for perceptual organization in the parietal cortex. *The Journal of*

Neuroscience, *38*(32), 7158–7169. https://doi.org/10.1523/JNEUROSCI.0436-18.2018

Gross, J., Kujala, J., Hamalainen, M., Timmermann, L., Schnitzler, A., & Salmelin, R. (2001). Dynamic imaging of coherent sources: Studying neural interactions in the human brain. *Proceedings of the National Academy of Sciences of the United States of America*, *98*(2), 694–699. https://doi.org/10.1073/pnas.98.2.694

Helfrich, R. F., Knepper, H., Nolte, G., Sengelmann, M., Konig, P., Schneider, T. R., & Engel, A. K. (2016). Spectral fingerprints of large-scale cortical dynamics during ambiguous motion perception. *Human Brain Mapping*, *37*(11), 4099–4111. https://doi.org/10.1002/hbm.23298

Holmes, C. J., Hoge, R., Collins, L., Woods, R., Toga, A. W., & Evans, A. C. (1998). Enhancement of MR images using registration for signal averaging. *Journal of Computer Assisted Tomography*, *22*(2), 324–333. https://doi.org/10.1097/00004728-199803000-00032

Honkanen, R., Rouhinen, S., Wang, S. H., Palva, J. M., & Palva, S. (2015). Gamma oscillations underlie the maintenance of feature-specific information and the contents of visual working memory. *Cerebral Cortex*, *25*(10), 3788–3801. https://doi.org/10.1093/cercor/bhu263

Hoogenboom, N., Schoffelen, J. M., Oostenveld, R., Parkes, L. M., & Fries, P. (2006). Localizing human visual gamma-band activity in frequency, time and space. *NeuroImage*, *29*(3), 764–773. https://doi.org/10.1016/j.neuroimage.2005.08.043

Huang, T., Chen, X., Jiang, J., Zhen, Z., & Liu, J. (2019). A probabilistic atlas of the human motion complex built from large-scale functional localizer data. *Human Brain Mapping*, *40*(12), 3475–3487. https://doi.org/10.1002/hbm.24610

Hupe, J. M., & Pressnitzer, D. (2012). The initial phase of auditory and visual scene analysis. *Philosophical Transactions of the Royal Society of London. Series B, Biological Sciences*, *367*(1591), 942–953. https://doi.org/10.1098/rstb.2011.0368

Hupe, J. M., & Rubin, N. (2003). The dynamics of bi-stable alternation in ambiguous motion displays: A fresh look at plaids. *Vision Research*, *43*(5), 531–548.

Jensen, O., Gips, B., Bergmann, T. O., & Bonnefond, M. (2014). Temporal coding organized by coupled alpha and gamma oscillations prioritize visual processing. *Trends in Neurosciences*, *37*(7), 357–369. https://doi.org/10.1016/j.tins.2014.04.001

Kanai, R., Carmel, D., Bahrami, B., & Rees, G. (2011). Structural and functional fractionation of right superior parietal cortex in bistable perception. *Current Biology*, *21*(3), R106–R107. https://doi.org/10.1016/j.cub.2010.12.009

Kanai, R., & Rees, G. (2011). The structural basis of inter-individual differences in human behaviour and cognition. *Nature Reviews. Neuroscience*, *12*(4), 231–242. https://doi.org/10.1038/nrn3000

Kayser, C., Salazar, R. F., & Konig, P. (2003). Responses to natural scenes in cat V1. *Journal of Neurophysiology*, *90*(3), 1910–1920. https://doi.org/10.1152/jn.00195.2003

Keil, A., Muller, M. M., Ray, W. J., Gruber, T., & Elbert, T. (1999). Human gamma band activity and perception of a gestalt. *The Journal of Neuroscience*, *19*(16), 7152–7161.

Klimesch, W. (2012). Alpha-band oscillations, attention, and controlled access to stored information. *Trends in Cognitive Sciences*, *16*(12), 606–617. https://doi.org/10.1016/j.tics.2012.10.007

Klimesch, W., Sauseng, P., & Hanslmayr, S. (2007). EEG alpha oscillations: The inhibition-timing hypothesis. *Brain Research Reviews*, *53*(1), 63–88. https://doi.org/10.1016/j.brainresrev.2006.06.003

Leech, R., Braga, R., & Sharp, D. J. (2012). Echoes of the brain within the posterior cingulate cortex. *The Journal of Neuroscience*, *32*(1), 215–222. https://doi.org/10.1523/JNEUROSCI.3689-11.2012

Leopold, D. A., & Logothetis, N. K. (1999). Multistable phenomena: Changing views in perception. *Trends in Cognitive Sciences*, *3*(7), 254–264.

Liaci, E., Bach, M., Tebartz van Elst, L., Heinrich, S. P., & Kornmeier, J. (2016). Ambiguity in tactile apparent motion perception. *PLoS One*, *11*(5), e0152736. https://doi.org/10.1371/journal.pone.0152736

Liaw, G. J., Kim, S., & Alais, D. (2022). Direction-selective modulation of visual motion rivalry by collocated tactile motion. *Attention, Perception, & Psychophysics*, *84*(3), 899–914. https://doi.org/10.3758/s13414-022-02453-y

Liu, L., Wang, F., Zhou, K., Ding, N., & Luo, H. (2017). Perceptual integration rapidly activates dorsal visual pathway to guide local processing in early visual areas. *PLoS Biology*, *15*(11), e2003646. https://doi.org/10.1371/journal.pbio.2003646

Logothetis, N. K. (2003). The underpinnings of the BOLD functional magnetic resonance imaging signal. *The Journal of Neuroscience*, *23*(10), 3963–3971.

Long, G. M., & Toppino, T. C. (2004). Enduring interest in perceptual ambiguity: Alternating views of reversible figures. *Psychological Bulletin*, *130*(5), 748–768. https://doi.org/10.1037/0033-2909.130.5.748

Maris, E., & Oostenveld, R. (2007). Nonparametric statistical testing of EEG- and MEG-data. *Journal of Neuroscience Methods*, *164*(1), 177–190. https://doi.org/10.1016/j.jneumeth.2007.03.024

Megumi, F., Bahrami, B., Kanai, R., & Rees, G. (2015). Brain activity dynamics in human parietal regions during spontaneous switches in bistable perception. *NeuroImage*, *107*, 190–197. https://doi.org/10.1016/j.neuroimage.2014.12.018

Melloni, L., Molina, C., Pena, M., Torres, D., Singer, W., & Rodriguez, E. (2007). Synchronization of neural activity across cortical areas correlates with conscious perception. *The Journal of Neuroscience*, *27*(11), 2858–2865. https://doi.org/10.1523/JNEUROSCI.4623-06.2007

Michalareas, G., Vezoli, J., van Pelt, S., Schoffelen, J. M., Kennedy, H., & Fries, P. (2016). Alpha-beta and gamma rhythms subserve feedback and feedforward influences among human visual cortical areas. *Neuron*, *89*(2), 384–397. https://doi.org/10.1016/j.neuron.2015.12.018

Mima, T., Oluwatimilehin, T., Hiraoka, T., & Hallett, M. (2001). Transient interhemispheric neuronal synchrony correlates with object recognition. *The Journal of Neuroscience*, *21*(11), 3942–3948.

Muckli, L., Kohler, A., Kriegeskorte, N., & Singer, W. (2005). Primary visual cortex activity along the apparent-motion trace reflects illusory perception. *PLoS Biology*, *3*(8), e265. https://doi.org/10.1371/journal.pbio.0030265

Muthukumaraswamy, S. D., & Singh, K. D. (2013). Visual gamma oscillations: The effects of stimulus type, visual field coverage and stimulus motion on MEG and EEG recordings. *NeuroImage*, *69*, 223–230. https://doi.org/10.1016/j.neuroimage.2012.12.038

Oostenveld, R., Fries, P., Maris, E., & Schoffelen, J. M. (2011). FieldTrip: Open source software for advanced analysis of MEG, EEG, and invasive electrophysiological data. *Computational Intelligence and Neuroscience*, *2011*, 156869. https://doi.org/10.1155/2011/156869

Piantoni, G., Kline, K. A., & Eagleman, D. M. (2010). Beta oscillations correlate with the probability of perceiving rivalrous visual stimuli. *Journal of Vision*, *10*(13), 18. https://doi.org/10.1167/10.13.18

Piantoni, G., Romeijn, N., Gomez-Herrero, G., Van Der Werf, Y. D., & Van Someren, E. J. W. (2017). Alpha power predicts persistence of bistable perception. *Scientific Reports*, *7*(1), 5208. https://doi.org/10.1038/s41598-017-05610-8

Pressnitzer, D., & Hupe, J. M. (2006). Temporal dynamics of auditory and visual bistability reveal common principles of perceptual organization. *Current Biology*, *16*(13), 1351–1357. https://doi.org/10.1016/j.cub.2006.05.054

Ray, S., & Maunsell, J. H. (2011). Different origins of gamma rhythm and high-gamma activity in macaque visual cortex. *PLoS Biology*, *9*(4), e1000610. https://doi.org/10.1371/journal.pbio.1000610

Rodriguez, E., George, N., Lachaux, J. P., Martinerie, J., Renault, B., & Varela, F. J. (1999). Perception's shadow: Long-distance synchronization of human brain activity. *Nature*, *397*(6718), 430–433. https://doi.org/10.1038/17120

Roelfsema, P. R. (2023). Solving the binding problem: Assemblies form when neurons enhance their firing rate-they don't need to oscillate or synchronize. *Neuron*, *111*(7), 1003–1019. https://doi.org/10.1016/j.neuron.2023.03.016

Rose, M., & Buchel, C. (2005). Neural coupling binds visual tokens to moving stimuli. *The Journal of Neuroscience*, *25*(44), 10101–10104. https://doi.org/10.1523/JNEUROSCI.2998-05.2005

Roy, A. V., Jamison, K. W., He, S., Engel, S. A., & He, B. (2017). Deactivation in the posterior mid-cingulate cortex reflects perceptual transitions during binocular rivalry: Evidence from simultaneous EEG-fMRI. *NeuroImage*, *152*, 1–11. https://doi.org/10.1016/j.neuroimage.2017.02.041

Schwartz, J. L., Grimault, N., Hupe, J. M., Moore, B. C., & Pressnitzer, D. (2012). Multistability in perception: Binding sensory modalities, an overview. *Philosophical Transactions of the Royal Society of London. Series B, Biological Sciences*, *367*(1591), 896–905. https://doi.org/10.1098/rstb.2011.0254

Schwarzkopf, D. S., Sterzer, P., & Rees, G. (2011). Decoding of coherent but not incoherent motion signals in early dorsal visual cortex. *NeuroImage*, *56*(2), 688–698. https://doi.org/10.1016/j.neuroimage.2010.04.011

Scocchia, L., Valsecchi, M., & Triesch, J. (2014). Top-down influences on ambiguous perception: The role of stable and transient states of the observer. *Frontiers in Human Neuroscience*, *8*, 979. https://doi.org/10.3389/fnhum.2014.00979

Seymour, K., Clifford, C. W., Logothetis, N. K., & Bartels, A. (2009). The coding of color, motion, and their conjunction in the human visual cortex. *Current Biology*, *19*(3), 177–183. https://doi.org/10.1016/j.cub.2008.12.050

Siegel, M., Donner, T. H., & Engel, A. K. (2012). Spectral fingerprints of large-scale neuronal interactions. *Nature Reviews. Neuroscience*, *13*(2), 121–134. https://doi.org/10.1038/nrn3137

Siegel, M., Donner, T. H., Oostenveld, R., Fries, P., & Engel, A. K. (2007). High-frequency activity in human visual cortex is modulated by visual motion strength. *Cerebral Cortex*, *17*(3), 732–741. https://doi.org/10.1093/cercor/bhk025

Sousa, T., Duarte, J. V., Costa, G. N., Kemper, V. G., Martins, R., Goebel, R., & Castelo-Branco, M. (2021). The dual nature of the BOLD signal: Responses in visual area hMT+ reflect both input properties and perceptual decision. *Human Brain Mapping*, *42*, 1920–1929. https://doi.org/10.1002/hbm.25339

Sterzer, P., Kleinschmidt, A., & Rees, G. (2009). The neural bases of multistable perception. *Trends in Cognitive Sciences*, *13*(7), 310–318. https://doi.org/10.1016/j.tics.2009.04.006

Stolk, A., Griffin, S., van der Meij, R., Dewar, C., Saez, I., Lin, J. J., Piantoni, G., Schoffelen, J. M., Knight, R. T., & Oostenveld, R. (2018). Integrated analysis of anatomical and electrophysiological human intracranial data. *Nature Protocols*, *13*(7), 1699–1723. https://doi.org/10.1038/s41596-018-0009-6

Sun, S., Zhen, S., Fu, Z., Wu, D. A., Shimojo, S., Adolphs, R., & Wang, S. (2017). Decision ambiguity is mediated by a late positive potential originating from cingulate cortex. *NeuroImage*, *157*, 400–414. https://doi.org/10.1016/j.neuroimage.2017.06.003

Tallon-Baudry, C., & Bertrand, O. (1999). Oscillatory gamma activity in humans and its role in object representation. *Trends in Cognitive Sciences*, *3*(4), 151–162. https://doi.org/10.1016/s1364-6613(99)01299-1

Thut, G., Nietzel, A., Brandt, S. A., & Pascual-Leone, A. (2006). Alpha-band electroencephalographic activity over occipital cortex indexes visuospatial attention bias and predicts visual target detection. *The Journal of Neuroscience*, *26*(37), 9494–9502. https://doi.org/10.1523/JNEUROSCI.0875-06.2006

van Dijk, H., Schoffelen, J. M., Oostenveld, R., & Jensen, O. (2008). Prestimulus oscillatory activity in the alpha band predicts visual discrimination ability. *The Journal of Neuroscience*, *28*(8), 1816–1823. https://doi.org/10.1523/JNEUROSCI.1853-07.2008

van Kerkoerle, T., Self, M. W., Dagnino, B., Gariel-Mathis, M. A., Poort, J., van der Togt, C., & Roelfsema, P. R. (2014). Alpha and gamma oscillations characterize feedback and feedforward processing in monkey visual cortex. *Proceedings of the National Academy of Sciences of the United States of America*, *111*(40), 14332–14341. https://doi.org/10.1073/pnas.1402773111

Wallach, H. (1935). Uber visuell wahrgenommene Bewegungsrichtung. *Psychologische Forschung*, *20*, 325–380.

Wang, L., Mruczek, R. E., Arcaro, M. J., & Kastner, S. (2015). Probabilistic maps of visual topography in human cortex. *Cerebral Cortex*, *25*(10), 3911–3931. https://doi.org/10.1093/cercor/bhu277

Weilnhammer, V., Stuke, H., Hesselmann, G., Sterzer, P., & Schmack, K. (2017). A predictive coding account of bistable perception - a model-based fMRI study. *PLoS Computational Biology*, *13*(5), e1005536. https://doi.org/10.1371/journal.pcbi.1005536

Wuerger, S., Shapley, R., & Rubin, N. (1996). "On the visually perceived direction of motion" by Hans Wallach: 60 years later. *Perception*, *25*(11), 1317–1318. https://doi.org/10.1068/P251317

Zaretskaya, N., Anstis, S., & Bartels, A. (2013). Parietal cortex mediates conscious perception of illusory gestalt. *The Journal of Neuroscience*, *33*(2), 523–531. https://doi.org/10.1523/JNEUROSCI.2905-12.2013

Zaretskaya, N., & Bartels, A. (2015). Gestalt perception is associated with reduced parietal beta oscillations. *NeuroImage*, *112*, 61–69. https://doi.org/10.1016/j.neuroimage.2015.02.049

Zhang, Y., Zhang, Y., Cai, P., Luo, H., & Fang, F. (2019). The causal role of alpha-oscillations in feature binding. *Proceedings of the National Academy of Sciences of the United States of America*, *116*(34), 17023–17028. https://doi.org/10.1073/pnas.1904160116

SUPPORTING INFORMATION

Additional supporting information can be found online in the Supporting Information section at the end of this article.

How to cite this article: Costa, G. N., Schaum, M., Duarte, J. V., Martins, R., Duarte, I. C., Castelhano, J., Wibral, M., & Castelo-Branco, M. (2024). Distinct oscillatory patterns differentiate between segregation and integration processes in perceptual grouping. *Human Brain Mapping*, *45*(12), e26779. https://doi.org/10.1002/hbm.26779